ChemPubSoc Europe

DOI: 10.1002/ejic.201900716

EurJIC European Journal of Inorganic Chemistry

Full Paper

Zr and Hf Complexes

Formation and Activation of Zr/Hf Bis(phenolate-ether) Precatalysts

Eric N. T. Cuthbert,[a,b] Vincenzo Busico,[b,c] David E. Herbert,[a] and Peter H. M. Budzelaar*[a,b,c]

Abstract: Zr and Hf complexes of bis(phenolate-ether) ("O4") ligands feature high activity, stereoselectivity and molecular weight capability for propene polymerization at high temperature. Here we report a simplified ligand synthesis and several new examples of O4 ligands. The formation of precatalysts **L**MR_2 (M = Zr, Hf; R = Bn, Me) from **L**H_2 and MR_4 was found to be accompanied in some cases by the formation of dimers $(\mu\text{-L})_2[MR_2]_2$, and X-ray structures of two such dimers have been determined. Treatment of **L**MMe_2 with $[Ph_3C]^+[B(C_6F_5)_4]^-$ produces fairly clean cationic species **L**MMe^+ which were studied by ^{1}H NMR. 2D ROESY data, in particular, suggest that for "smaller" O4 ligands the **L**MMe^+ cation reversibly rearranges from the active (*fac*/*fac*) form to a presumably inactive *fac*/*mer* or *mer*/*mer* form; more bulky substituents appear to suppress this rearrangement. Implications for polymerization catalysis are discussed.

Introduction

Polyolefins are extremely versatile materials, finding ever-expanding areas of application in part due to the development of new grades prepared using increasingly sophisticated catalytic systems.[1] Industrial polypropylene production is still dominated by heterogeneous Ziegler-Natta catalysts, which can produce highly stereoregular polymers at high operating temperatures.[2] Zr and Hf bis(phenolate-ether) catalysts (here designated as O4 catalysts; see Figure 1), originally patented by SYMYX[3] and later acquired by Dow,[4] comprise one of few homogeneous catalyst classes capable of working at high temperatures while still maintaining a high molecular weight capability. Based in part on X-ray structures of **L**MCl_2 and **L**MBn_2 catalyst precursors,[3,5] and also on similarity to ONNO[6] and OSSO[7] systems, the active species in O4 systems is believed to have an octahedral coordination geometry with the O4 ligand coordinated in a *fac*/*fac* C_2-symmetric fashion around the metal, leaving two mutually *cis* sites available for the growing chain and incoming monomer.[8]

While this is a plausible scenario, it should be noted that the situation in ONNO systems is complicated by ligand skeletal rearrangement from *fac*/*fac* to *mer*/*mer* (Figure 2), with important consequences for catalyst activity;[9] there appears to be no *a priori* reason why the same could not apply to O4 type catalysts.

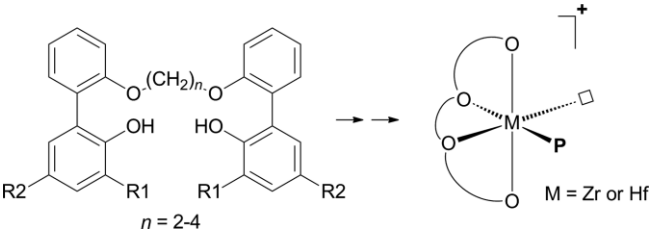

Figure 1. Representative O4 ligand structure and proposed active species.

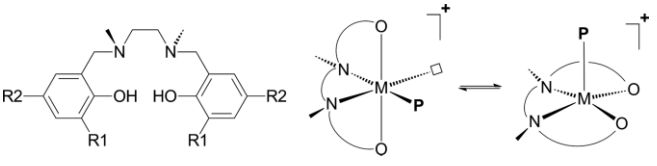

Figure 2. The ONNO ligand[6] and its active species equilibrium.[9b]

In the present work, we present the results of a combined NMR and computational (density functional) study of selected activated O4 catalysts, finding that most likely conformational changes occur in some O4 systems as well. In addition, we report evidence that even the "standard" synthesis of precursor complexes **L**MBn_2 and **L**MMe_2 is less than straightforward: depending on the choice of ligand and reaction conditions, treatment of **L**H_2 with MBn_4 or MMe_4 can produce both monomeric **L**MR_2 and dimeric $(\mu\text{-L})_2[MR_2]_2$ compounds. Implications for testing of catalyst performance are discussed.

Results and Discussion

Ligand Synthesis

Ligands were mostly synthesized according to adaptations of procedures published by Symyx/Waymouth[3,5a] and Dow;[4]

[a] *Department of Chemistry, University of Manitoba, 144 Dysart Road, Winnipeg MB R3T 2N2, Canada*
[b] *Dutch Polymer Institute (DPI), P.O. Box 902, 5600 AX Eindhoven, The Netherlands*
[c] *Dipartimento di Scienze Chimiche, Università di Napoli 'Federico II', Via Cintia, 80126 Napoli, Italy*
E-mail: p.budzelaar@unina.it

Supporting information and ORCID(s) from the author(s) for this article are available on the WWW under https://doi.org/10.1002/ejic.201900716.

precise details can be found in the Supporting Information for all ligands and intermediates studied. Scheme 1 shows the numerous protection/deprotection steps required in the original Symyx scheme (method **A**) which ultimately reduces overall yield. The Dow method (Scheme 2, method **B**) reduces the number of steps by employing THP as a phenol protecting group; *ortho*-directed lithiation and simpler deprotection procedures are highly advantageous here but may experience problems if R contains competing directing groups such as fluorine atoms. We found that while more effective than the lengthy method **A**, the *i*PrOBPin required for **12** in method **B** often formed emulsions during work-up, which complicated extraction procedures and reduced yields. As an alternative, we add anhydrous $ZnCl_2$ after *n*BuLi addition to **11**, converting this *in situ* into an organozinc compound (**13**) for immediate Negishi coupling (Scheme 2, method **B′**). This not only avoids the emulsion problems but saves a step in the synthesis of the final ligand. A total of 20 O4 ligands were synthesized by these three methods (Figure 3).

The ligands are separated into the groups 2C, 3C and 4C, corresponding to the length (i.e., the number of methylene units) of the alkyl chain linking the aryl ether donor groups. Substitution at the remaining phenolate *ortho* positions (R_1) allows investigation of the effect of steric bulk as well as electron-donating abilities. All ligands were characterized by ^1H and ^{13}C NMR, HRMS and selected ligands also by X-ray crystallography.

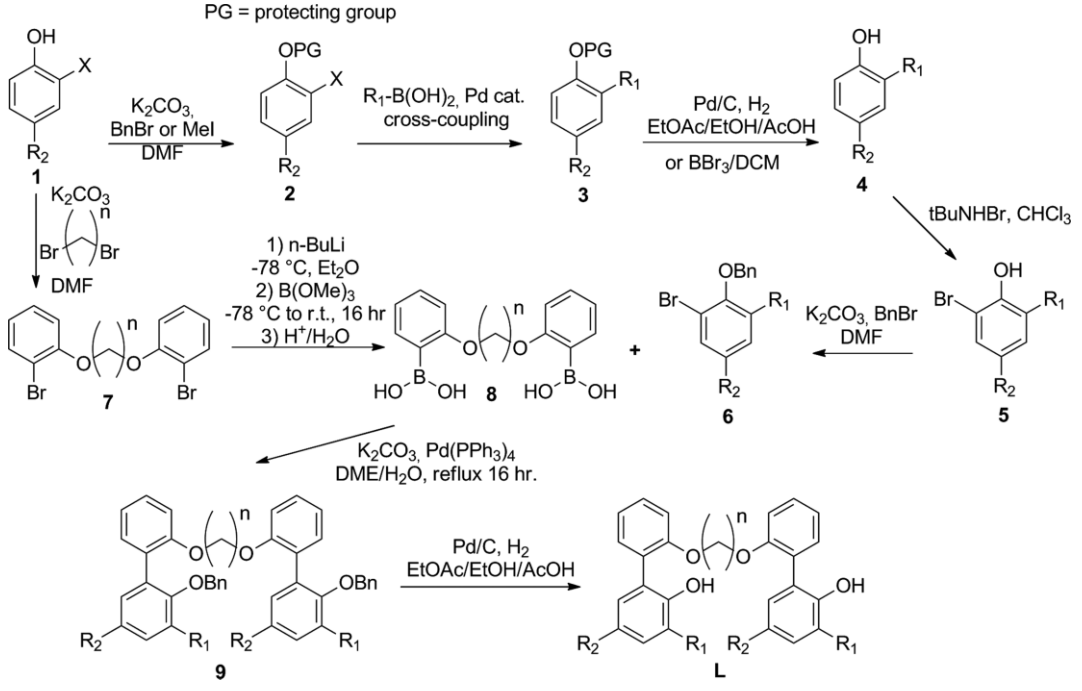

Scheme 1. Minor adaptations of Symyx/Waymouth O4 ligand synthesis (method **A**).[3,5a]

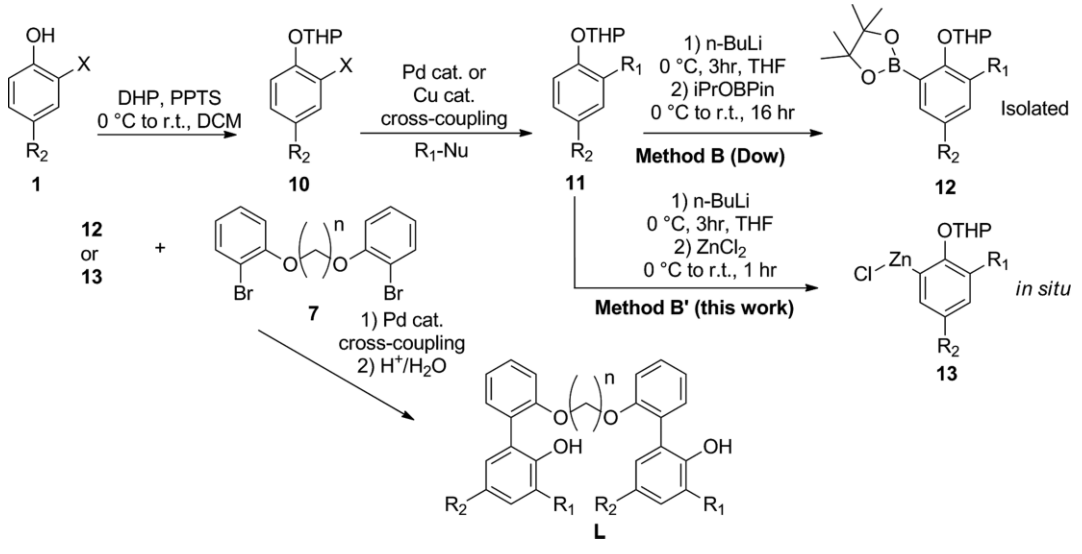

Scheme 2. Dow O4 ligand synthesis (method **B**)[4] and our adaptation (method **B′**).

R_1	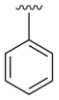		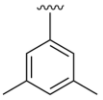	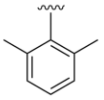	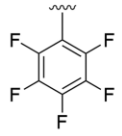	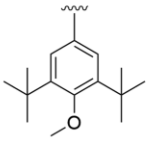	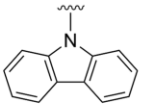	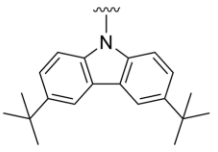
R_2	H	Me	H	H	H	H	H	H
n = 2	**L1**[a,b]	**L4**[a]	**L7**[b]	**L10**[a]	N/A	N/A	**L16**[c]	N/A
n = 3	**L2**[a,b,c]	**L5**[a]	**L8**[a,b]	**L11**[a]	**L13**[a]	N/A	**L17**[c]	**L19**[c]
n = 4	**L3**[c]	**L6**[a]	**L9**[a,b]	**L12**[a]	**L14**[a]	**L15**[b]	**L18**[c]	**L20**[c]

Figure 3. Synthesized ligand set. [a] Symyx/Waymouth method **A**. [b] Dow method **B**. [c] *in situ* Negishi reagent method **B'**.

We here survey formation of **L**MR_2 precatalysts from **L**H_2 and MR_4, and their activation to cations **L**MR^+, as a preliminary to exploring catalyst performance in propene polymerization.[10] Not all ligands were tested in each type of synthetic approach: in this paper, we describe representative results.

Synthesis of Precursors LMR_2

From LH_2 and MBn_4

Complexes **L**MBn_2 (M = Zr or Hf) are easily and conveniently generated from the free ligand **L**H_2 and commercially available MBn_4; this is a popular approach for post-metallocene type catalysts.[11] The complexes can be isolated and purified or generated *in situ* and used "as is" in catalyst testing: according to Waymouth, complex formation is clean and catalytic performance of isolated or *in situ* generated complexes is virtually identical.[5a]

In our hands, synthesis of all 2C complexes proceeded without problems. The reaction is complete within minutes at room temperature; ^{1}H NMR spectra of the crude mixture show sharp peaks and indicated the presence of a single complex with effective C_2 symmetry (Figure S1; **L1**$HfBn_2$ in Figure 4a). Layering

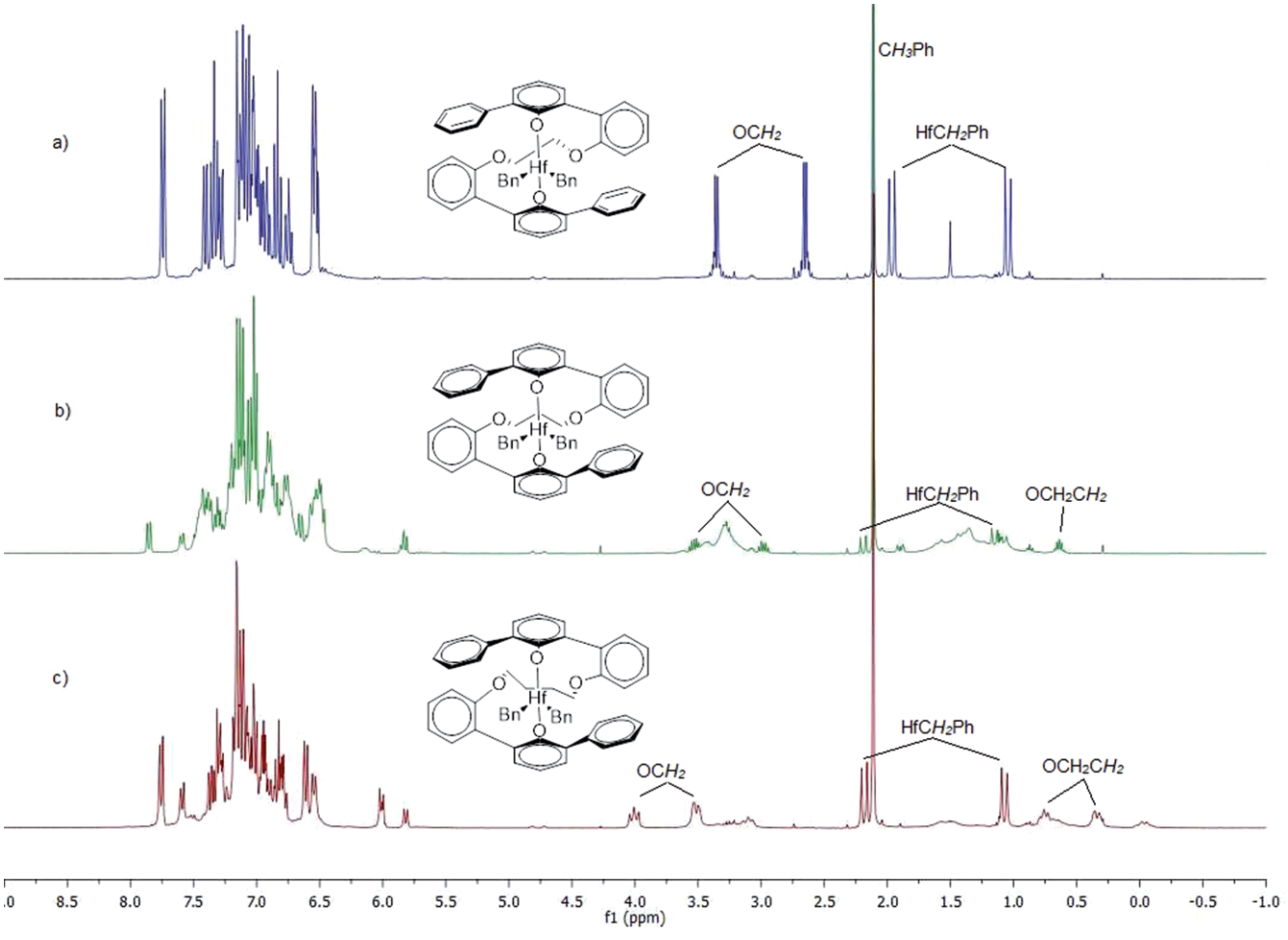

Figure 4. 300 MHz ^{1}H NMR spectra of *in situ* formed products from the reactions of a) **L1**H_2; b) **L2**H_2 and c) **L3**H_2 with $HfBn_4$ at 25 °C, [D_6]benzene.

of these samples with hexanes yielded in most cases X-ray quality crystals; the structures of two representative complexes (Figure 5) demonstrate the expected octahedral coordination environment of the metal.

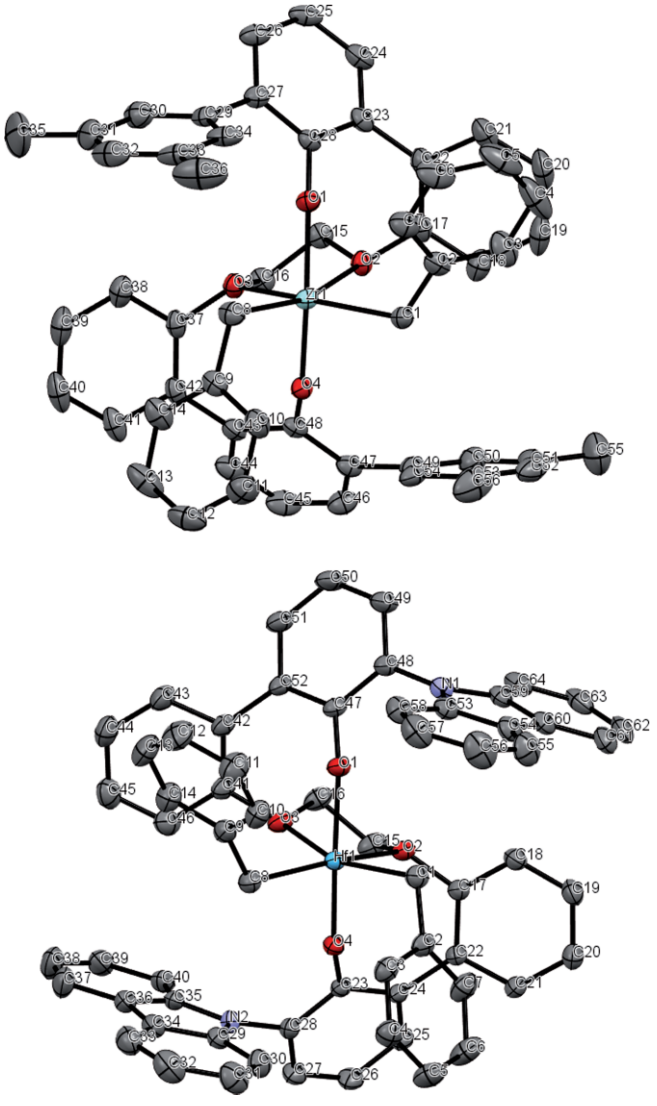

Figure 5. Thermal ellipsoid (50 %) plots for **L7**$ZrBn_2$ and **L16**$HfBn_2$; H atoms omitted for clarity.

Attempts using several 3C and 4C ligands produced rather different results as illustrated in Figure 4b/c (**L2**$HfBn_2$ and **L3**$HfBn_2$). Broad signals were observed in the ^{1}H NMR spectra of crude *in situ* reaction mixtures and also after work-up of the products, hinting at the presence of multiple species and/or fluxional behavior. Crystals grown from a solution of **L6**H_2/$ZrBn_4$ proved that the anticipated C_2-symmetric complex does indeed form (Figure 6) although the extent to which it does remains uncertain. More focused experiments revealed that broad spectra were obtained primarily when concentrations larger than 50 mM were used. When reactions were carried out at lower concentrations, the spectra of the products after work-up also were much cleaner. This is consistent with the report by Waymouth that apparently clean 4C Zr and Hf complexes were obtained when working at a concentration of ca. 10 mM, although these authors did not mention any concentration dependence.[5a]

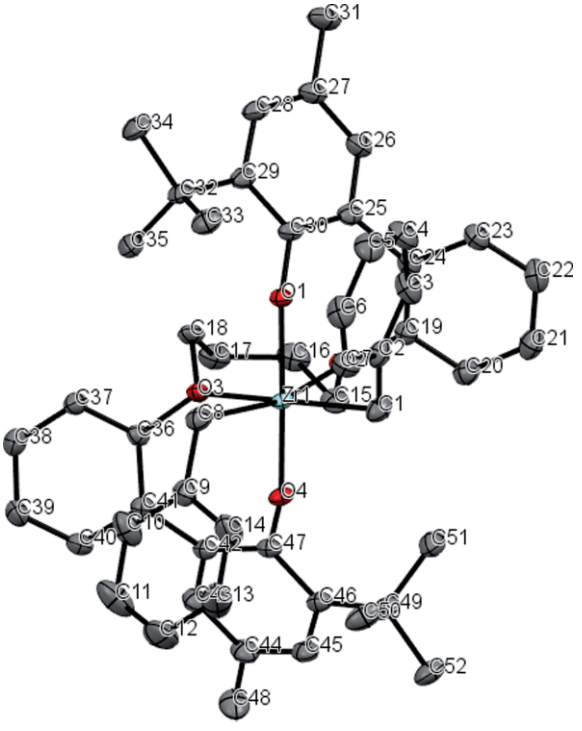

Figure 6. Thermal ellipsoid (50 %) plot for **L6**$ZrBn_2$; H atoms omitted for clarity.

The reaction temperature also affects the outcome of the reaction. This was checked for the reaction of $HfBn_4$ with 3C ligand **L2** (Figure 7). This reaction was carried out at –78 °C and at +65 °C, and subsequent NMR spectroscopy for both was performed at room temperature. The spectra differ greatly, the "sharp" component being nearly absent in the broadened spectrum of the low-temperature reaction product.

In separate experiments, X-ray quality crystals could be grown from reactions carried out at room temperature and at –35 °C. The former was found to be of the expected monomeric complex **L2**$HfBn_2$ while the latter unexpectedly turned out to be a dimer containing two bridging **L2** ligands (Figure 8).

Fairly pure (μ-**L2**)$_2$[$HfBn_2$]$_2$ was obtained by working at lower temperature and higher concentration during complexation. The resulting poorly soluble powder produces broad spectra both at room temperature and at elevated temperatures. While cooling of the sample to 10 °C sharpened the signals considerably, the spectra were never clean and clear enough for complete interpretation and assignment (Figure S2).

The above formation of a complex with two bridging ligands turns out not to be an isolated case. Spectra from the reaction of 4C ligand **L20**H_2 with $HfBn_4$ at –35 °C in [D_8]toluene featured both sharp and broad signals (Figure S3). Crystals obtained by layering hexanes also revealed the presence of a dimer with bridging O4 ligands (Figure 9).

Dinuclear ligand-bridged group IV precatalysts have precedent. The group of Agapie designed dinucleating (OONN)$_2$ li-

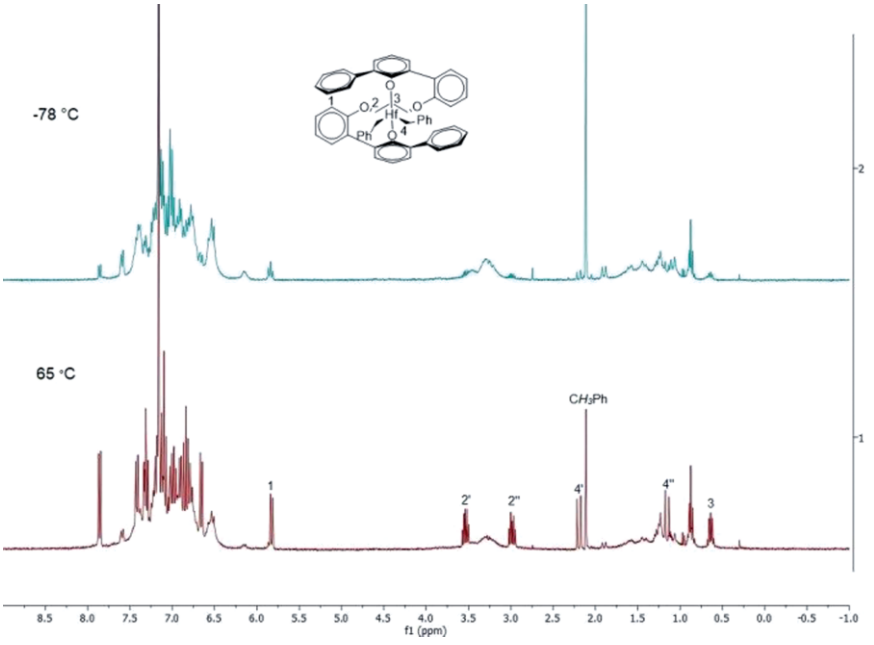

Figure 7. Room temperature 300 MHz ^{1}H NMR spectra of isolated "**L2**HfBn$_2$" generated from **L2**H$_2$ and HfBn$_4$ at −78 °C (top) and +65 °C (bottom).

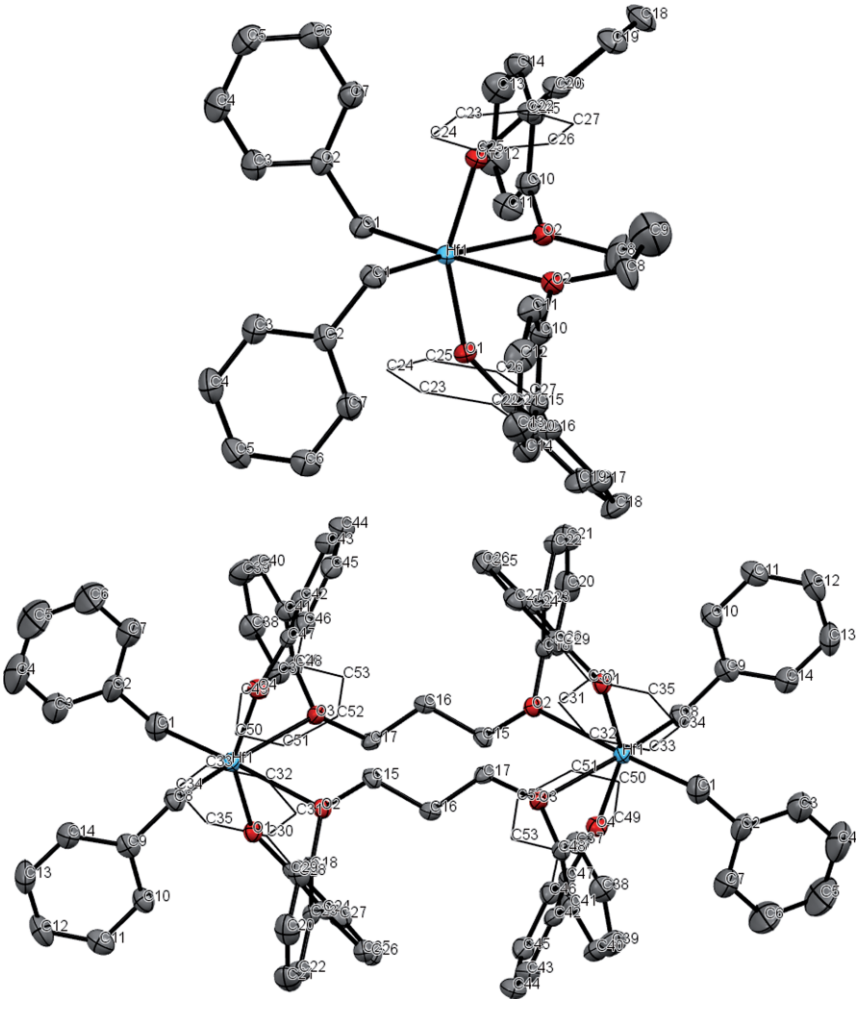

Figure 8. Thermal ellipsoid (50 %) plots for **L2**HfBn$_2$ and its dimer (μ-**L2**)$_2$[HfBn$_2$]$_2$. Solvent molecules, H atoms and a disordered carbon (C9) in **L2**HfBn$_2$ omitted for clarity; terminal phenyl groups are shown in stick style.

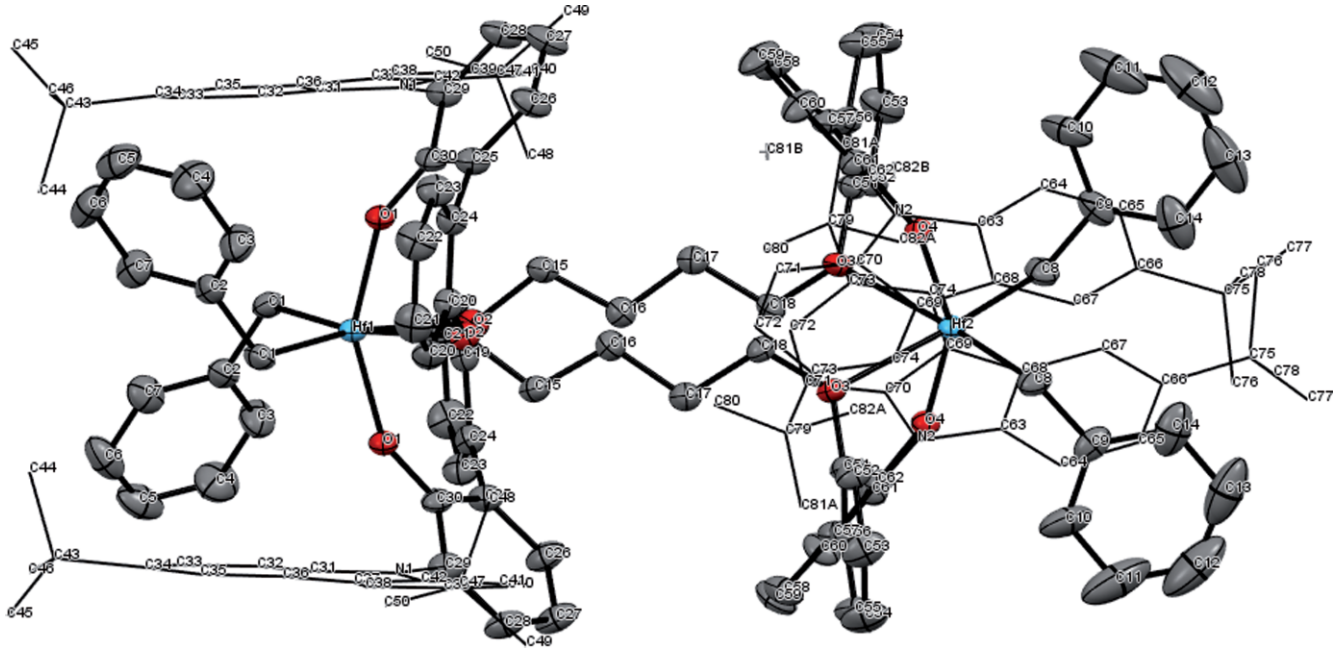

Figure 9. Thermal ellipsoid (50 %) plot for (μ-**L20**)$_2$[HfBn$_2$]$_2$; carbazolyl groups show in stick style and H atoms omitted for clarity.

gands where the ligand framework holds two octahedral active sites in close proximity and reported that the presence of a second metal site influences tacticity and comonomer incorporation.[11d,12] In contrast, the OSSO ligands mentioned above form dinuclear ligand-bridged Ti precatalyst complexes in which the two active sites point away from each other (similar to our dimers) but in which the Ti–S coordination has been lost.[7b] The present O4 dimer complexes are unusual in the sense that the environment of each site, formed from two phenolate-ether half-ligands, produces a coordination geometry very similar to that in the monomer complex where a single bis(phenolate-ether) ligand folds around the metal center.

From LH$_2$ and MMe$_4$

It is clear that the *in situ* formation of **L**MBn$_2$ from **L**H$_2$ and MBn$_4$ is not entirely without problems. Also, "activated" **L**MBn$^+$ species might not be representative of the true active species formed from O4 catalyst precursors, due to the diverse coordination possibilities of the remaining Bn group. We, therefore, turned to the synthesis of **L**MMe$_2$ precursors, following a procedure described in Dow patents.[2] In brief, MMe$_4$ is generated at low temperature from MCl$_4$ and MeMgBr in toluene, and the ligand **L**H$_2$ is added when the formation of MMe$_4$ is essentially complete; filtration and solvent removal leave a very pure crude product. A more detailed description is given in the experimental part.

Spectra obtained from these syntheses were generally much cleaner than those from MBn$_4$ reactions and showed no broadened signals. In most cases, the formation of a single product was indicated (Figure S4 shows an example) which contrasts with the challenging complexation and messy crude mixtures obtained from **L5**H$_2$ and ZrBn$_4$ (Figure S5). Figure 10 shows the structure of **L5**ZrMe$_2$ (crystals obtained directly by layering a benzene solution of very clean crude product with hexanes). This structure and several others (see the SI) demonstrate that the dimethyl complexes are monomeric and octahedral with exact or approximate C_2 symmetry in the solid state. All cases demonstrate shorter ligand–metal bond lengths on average for Hf relative to Zr, as has been observed previously for O4 complexes.[5a]

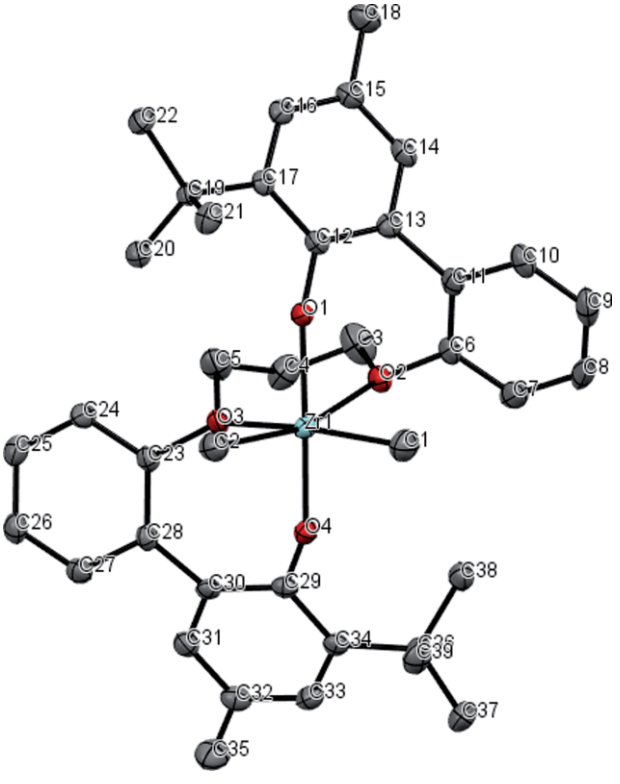

Figure 10. Thermal ellipsoid (50 %) plot for **L5**ZrMe$_2$; H atoms omitted for clarity.

However, for some of the more elaborate ligands (especially **L18** and **L20**), in combination with both $ZrMe_4$ and $HfMe_4$, a second set of sharp peaks was observed, indicating a second product (Figure 11). Diffusion NMR experiments on crude **L20**MMe_2 (see SI) revealed that for both metals the minority and majority species differ in hydrodynamic volume (spherical approximation) by a factor of 2.00 (Zr)/2.04 (Hf), strongly suggesting that the second product is the dimer (μ-**L**)$_2$[MMe_2]$_2$: dimer formation is therefore not restricted to the MBn_4 reactions.

NMR Study of [LMMe]$^+$[B(C_6F_5)$_4$]$^-$

Cationic complexes **L**MMe^+ were selected as models for the active species derived from O4 catalysts. Benzyl cations **L**MBn^+ were considered to be less representative in view of the diverse binding modes available to the benzyl group.[13]

The reaction of **L**MMe_2 with [Ph_3C]$^+$[B(C_6F_5)$_4$]$^-$ (TTFB) in [D_8]toluene was found to be clean for most ligands studied, and the resulting cationic complexes were fairly stable, the Hf

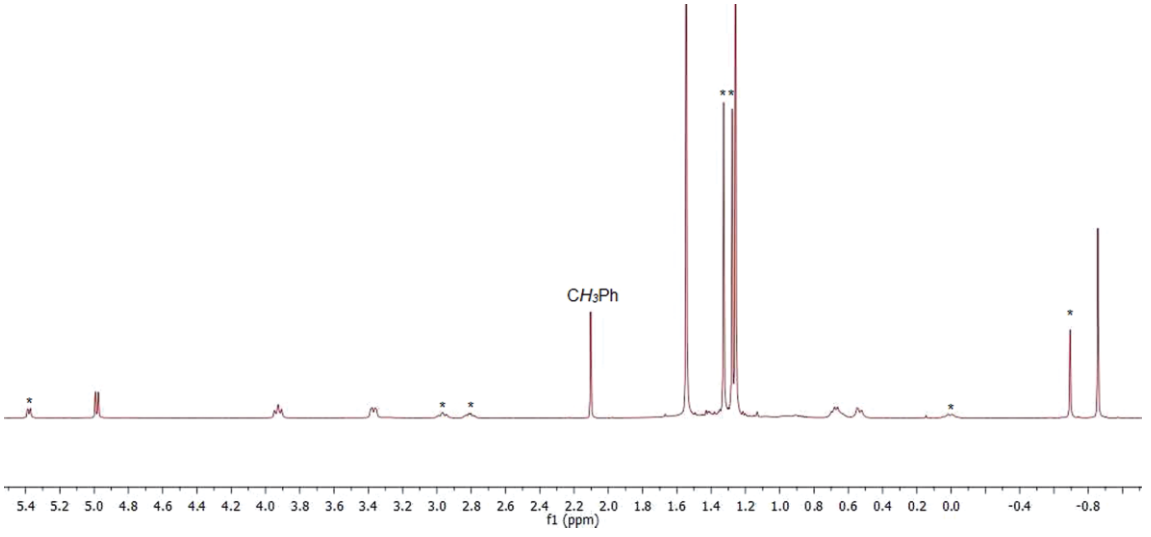

Figure 11. Section of the ^{1}H NMR spectrum of the crude product from the reaction of **L20**H_2 and $ZrMe_4$, in [D_6]benzene. Asterisks denote minority species signals.

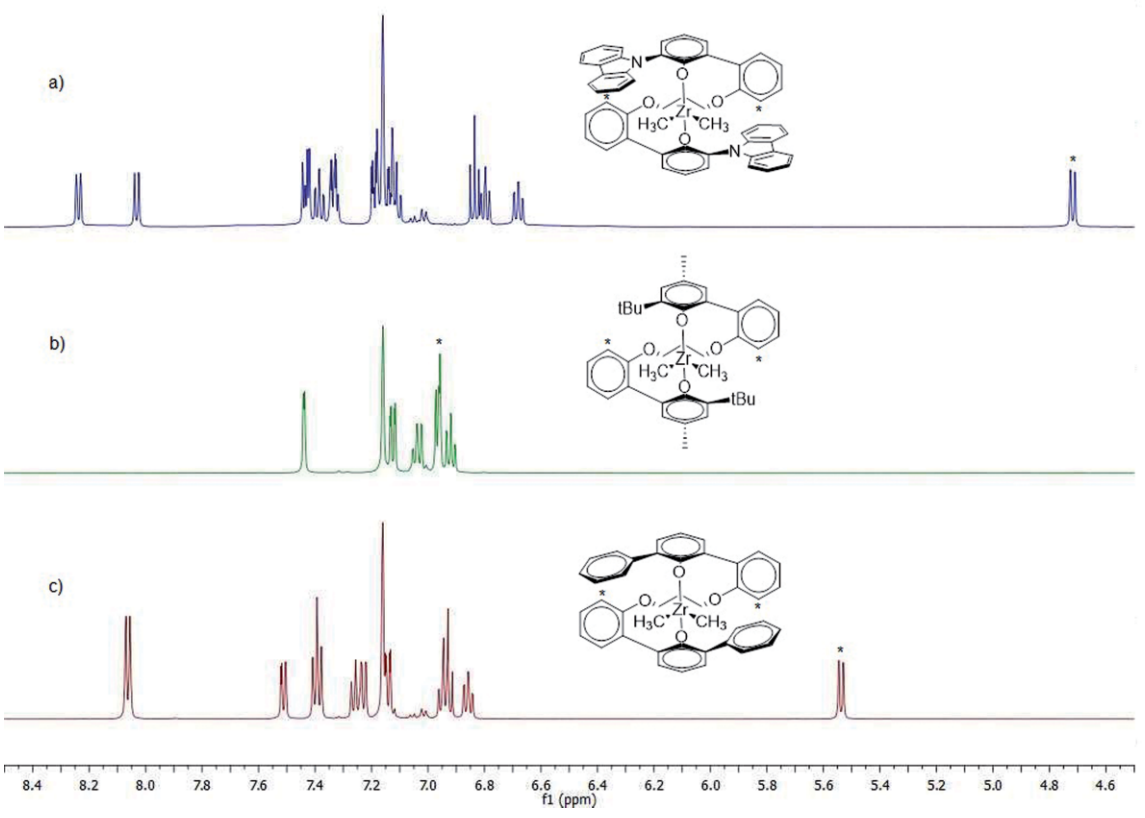

Figure 12. 500 MHz ^{1}H NMR aromatic regions of a) **L17**$ZrMe_2$; b) **L5**$ZrMe_2$ and c) **L2**$ZrMe_2$ complexes at 25 °C, [D_6]benzene.

complexes, in particular, surviving for some time at room temperature. Unfortunately, attempts to grow X-ray quality single crystals of any of these cations have so far been unsuccessful, so we must rely on NMR data (mostly ^{1}H 1D and 2D ROESY spectroscopy) for conformational information.

The aromatic regions of ^{1}H NMR spectra of even the simplest O4 catalyst precursors are extremely crowded, and complete assignment is challenging. However, many spectra of both **L**MMe$_2$ and **L**MMe$^+$ species show a clearly separated high-field resonance (below 6 ppm) for the arene hydrogen *ortho* to the aryl ether functionality (Figure 12a/c), that we believe is caused by its C-H bond pointing into the π-cloud of an aryl substituent *ortho* to the phenoxy group on the other end of the ligand (the "*o*-H signal", Figure 13).[14] In line with this hypothesis, such a high-field resonance is not observed for ligands lacking an aryl substituent in that position (e.g. **L5**, Figure 12b). Basic modeling shows that this type of ring current shielding should be absent or strongly diminished in *fac*/*mer* and *mer*/*mer* ligand conformations. We, therefore, believe that the presence of such high-field aromatic resonance can be taken as evidence that the ligand has assumed a *fac*/*fac* conformation. In addition, ROESY spectra involving the Me group(s) at the metal and the methylene groups of the ligand provide valuable 3D structural information. We here discuss spectra of Hf complexes of **L1**/**L2** and **L19** as typical examples of "small" and "large" ligands, respectively. Each species formed a dense, poorly-soluble orange oil upon activation which is consistent with the formation of [**L**MR]$^+$[B(C$_6$F$_5$)$_4$]$^-$ ion pairs.

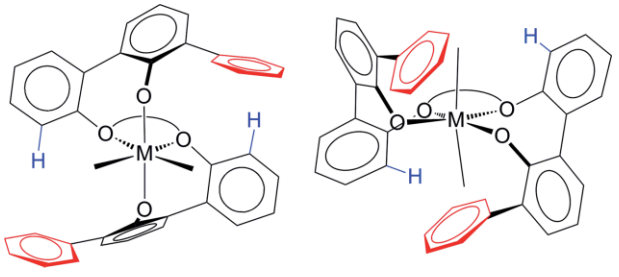

Figure 13. *fac*/*fac* and *mer*/*mer* structures for **L**MR$_2$. "*o*-H" protons are highlighted blue while aromatic rings that induce ring current shielding for the *o*-H protons are highlighted red.

L1HfMe$^+$

Activation of **L1**HfMe$_2$ produced NMR spectra that were broad and difficult to interpret (Figure 14b). However, the addition of one equivalent of OPPh$_3$ to this mixture slowly produced a new, major complex [**L1**HfMe•OPPh$_3$]$^+$[B(C$_6$F$_5$)$_4$]$^-$ that is stable at room temperature overnight in solution and yields sharper NMR spectra (Figure 14c). The presence of four separate ether protons in ^{1}H spectra (at 2.82–3.53 ppm) indicates that the complex is now C_1-symmetric while integration against the HfMe protons indicates abstraction of one methyl group from the precatalyst. A ^{31}P shift downfield from pure OPPh$_3$ indicates coordination of OPPh$_3$ to the electron-deficient Hf center while

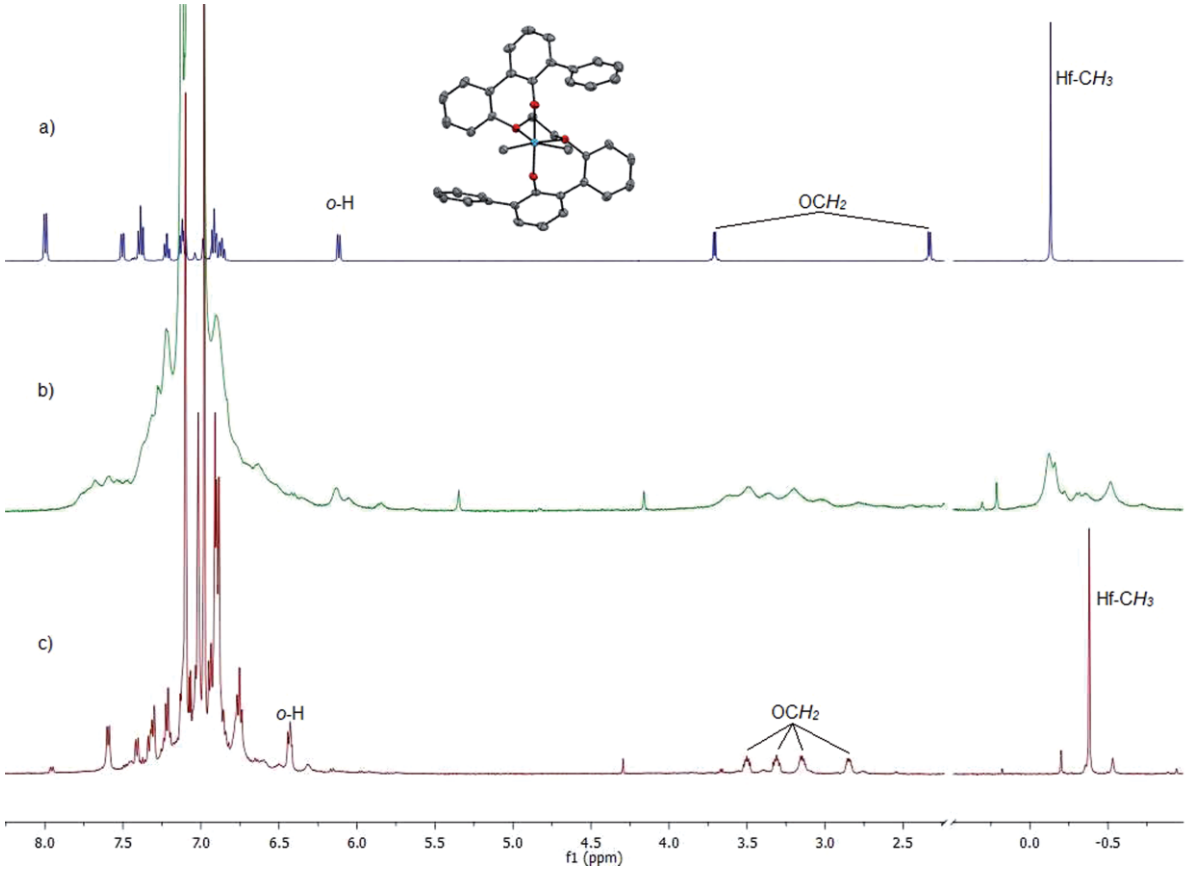

Figure 14. 500 MHz ^{1}H NMR spectra of a) **L1**HfMe$_2$ at −5 °C; b) [**L1**HfMe]$^+$[B(C$_6$F$_5$)$_4$]$^-$ at −5 °C and c) [**L1**HfMe•OPPh$_3$]$^+$[B(C$_6$F$_5$)$_4$]$^-$ at 25 °C, [D$_8$]toluene.

^{19}F spectra display similar chemical shifts and broadening as the activator, indicating loose and non-specific anion binding to the metal (Figure S6/S7).[13b,15] 2D ^{1}H-^{1}H ROESY data demonstrate behavior similar to that of the precursor **L1**$HfMe_2$, with no observable backbone-HfMe contact (Figure S8/S9). For these reasons, we believe that the $OPPh_3$ adduct is *fac*/*fac*, and this is supported by DFT calculations (below).

L2HfMe$^+$

Like its **L1**$HfMe^+$ analog, **L2**$HfMe^+$ generated by Me abstraction from **L2**$HfMe_2$ shows broad signals at room temperature (Figure 15b) although on cooling to –15 °C the spectrum becomes sharp (Figure 15c).

It shows a major component with a single Hf*Me* resonance (^{1}H: –0.06 ppm; ^{13}C: 51.1 ppm) as well as a minor component with Hf*Me* at somewhat higher field (^{1}H: –0.37 ppm; ^{13}C: 46.6 ppm; major/minor ca. 12:1; see also Figure S10). For the majority species, *two* separate *o*-H signals (1H each) can be observed, at more "normal" chemical shifts that indicate loss of the ring current effect mentioned above. The two ligand halves have become inequivalent, and the broadening observed at higher temperature likely represents a process exchanging these halves (see below). 2D ROESY spectra at 50 °C (Figure S11) demonstrate exchange between the majority and minority Hf-CH_3 species not observed at –15 °C (Figure S12).[16]

The loss of ring current shielding experienced by the *o*-H protons suggest that they are no longer directed into the phenyl substituents, which is most easily explained by a change in conformation, *e.g.*, to *fac*/*mer* or *mer*/*mer* as mentioned above. This is confirmed by 2D ROESY experiments (Figure S12), which show a contact between the Hf-CH_3 protons and backbone methylene protons that is incompatible with a *fac*/*fac* arrangement and is not observed in precursor **L2**$HfMe_2$ (Figure S13).

Based on the above, we suggest that the room temperature dynamic process involves a reversible switch between either *mer*/*mer* or *fac*/*mer* and *fac*/*fac* structures as well as a "back-skip" of the Hf*Me* group. One possible mechanism for this is summarized in Scheme 3.

As described above for [**L1**$HfMe]^+$, the cation [**L2**$HfMe]^+$ could be trapped as a $OPPh_3$ adduct. The ^{1}H NMR spectrum (Figure 15d) illustrates an upfield shift of the *o*-H signals upon $OPPh_3$ addition, more reminiscent of the **L2**$HfMe_2$ precursor (Figure 15a) which is *fac*/*fac* in structure. Also, in accord with a *fac*/*fac* conformation, the 2D ROESY spectrum of the adduct (Figure S14) does not show the contact between Hf-CH_3 and methylene protons observed for [**L2**$HfMe]^+[B(C_6F_5)_4]^-$. This suggests that, unlike the parent cation [**L2**$HfMe]^+$, the adduct [**L2**$HfMe{\cdot}OPPh_3]^+$ has a *fac*/*fac* structure.

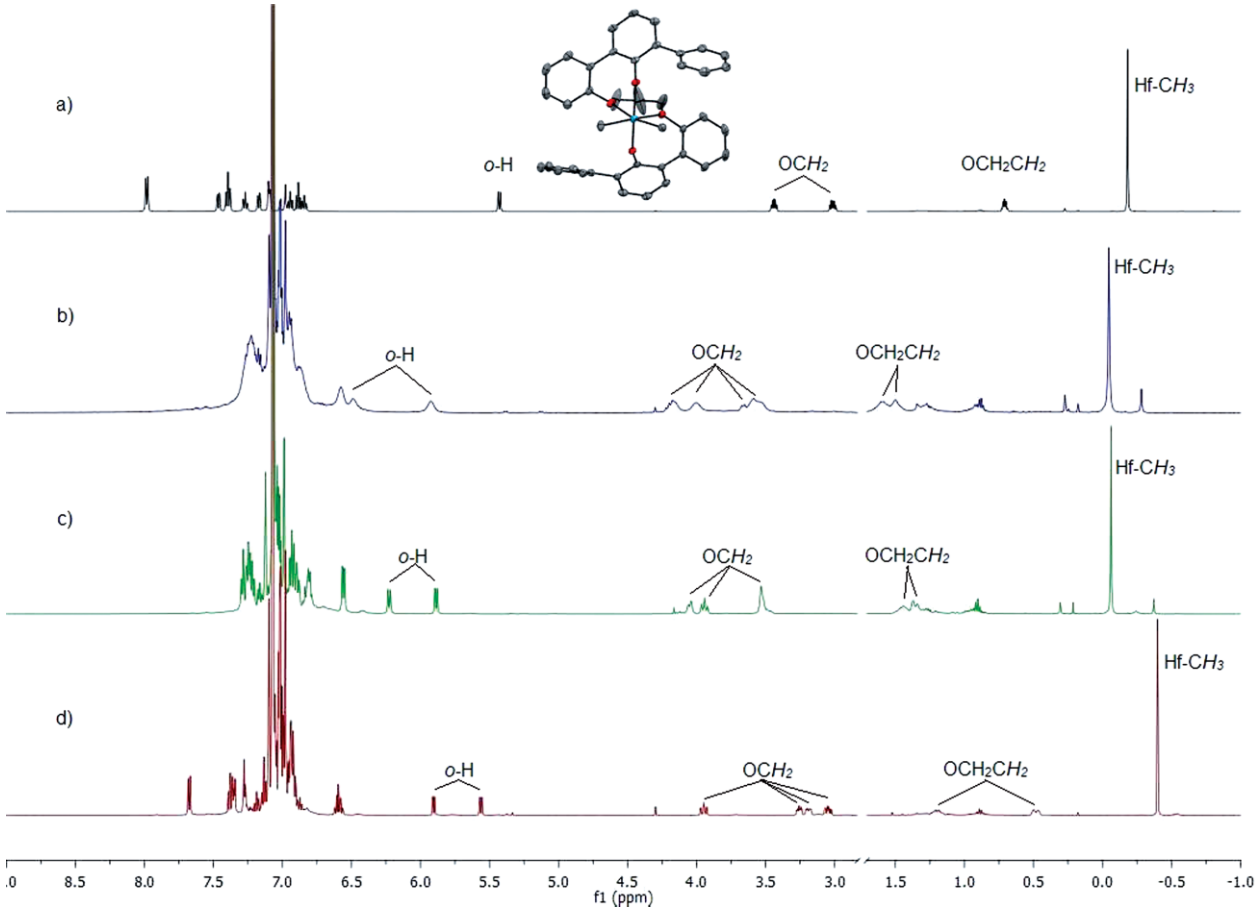

Figure 15. 500 MHz ^{1}H NMR spectra of a) **L2**$HfMe_2$ at 25 °C; b) [**L2**$HfMe]^+[B(C_6F_5)_4]^-$ at 25 °C; c) [**L2**$HfMe]^+[B(C_6F_5)_4]^-$ at –15 °C and d) [**L2**$HfMe{\cdot}OPPh_3]^+[B(C_6F_5)_4]^-$ at 25 °C, [D_8]toluene. Intense signals at ca. 7.05 ppm are due to side product CH_3CPh_3 aromatic protons, exacerbated by poor solubility of the ion pairs.

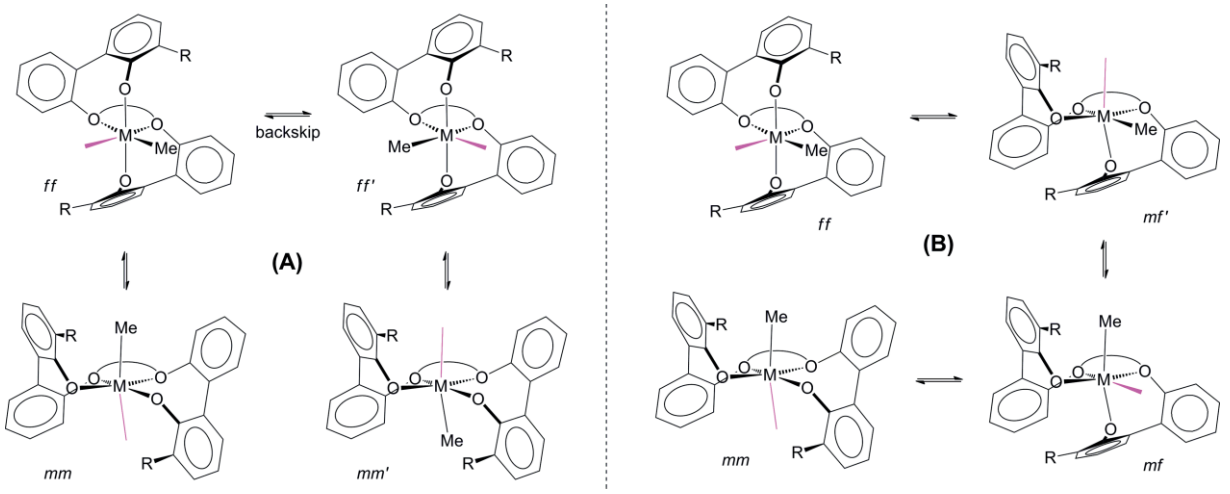

Scheme 3. Potential exchange mechanism in **L**MMe$^+$ cations: (A) exchange of ligand halves in *mer*/*mer* complex via *fac*/*fac* structure and backskip; (B) possible sequence of steps for the *fac*/*fac* to *mer*/*mer* isomerization assumed in (A).

L19HfMe$^+$

The reaction of **L19**HfMe$_2$ with TTFB (Figure 16a) also resulted in a rather clean formation of a cationic species, showing a single Hf-C*H*$_3$ group and inequivalent ligand halves. For this ligand, however, the *o*-H signals remain at high field (Figure 16c), and ROESY spectra do not show any contacts between the Hf-C*H*$_3$ and methylene protons (Figure S15). Additionally, the overall spectrum is very similar to **L19**HfMe$_2$ precursor although less symmetric, suggesting strongly that for this system the ligand keeps its *fac*/*fac* arrangement also in the activated species.

L19 HfMe$^+$ is fluxional at room temperature, suggesting an exchange of the two ligand halves. Since the ligand is already in the *fac*/*fac* conformation, only the top back-skip part of Scheme 3 (A) is needed to explain the exchange.

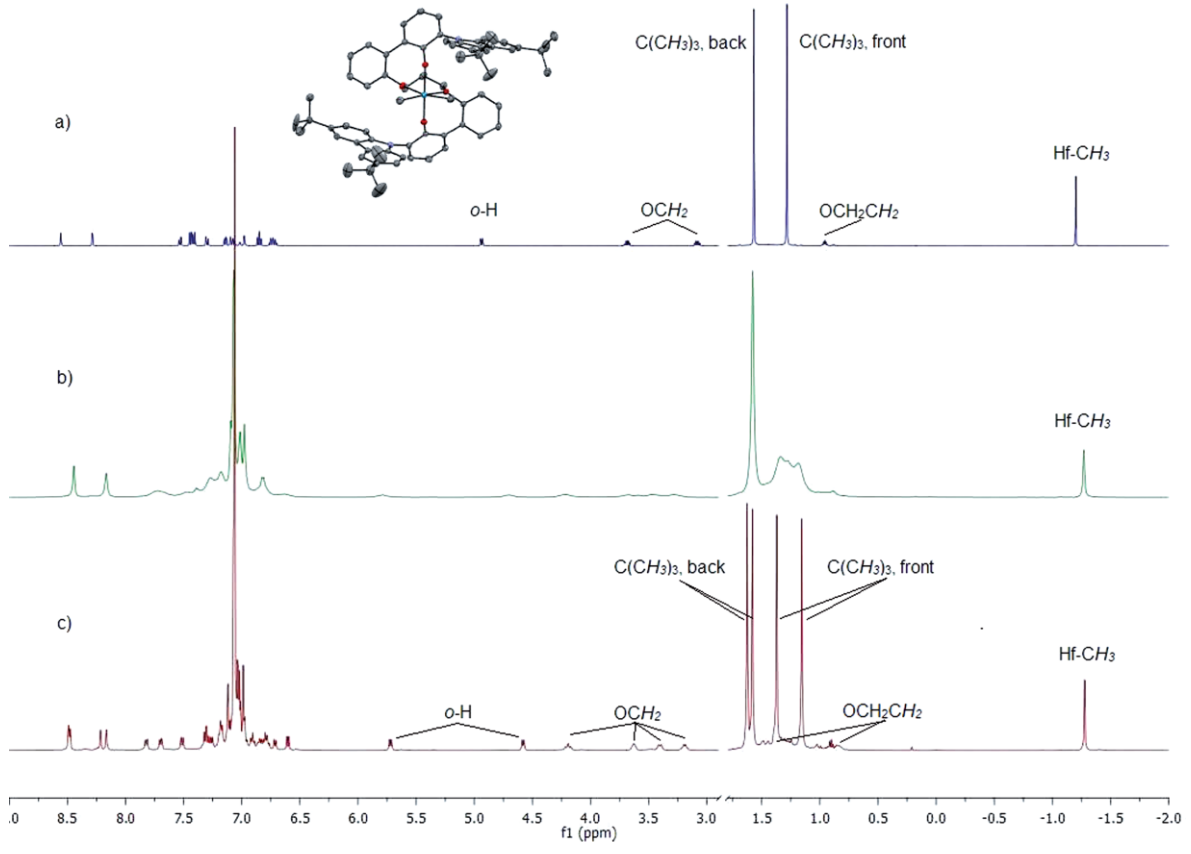

Figure 16. 500 MHz ^{1}H NMR spectra of a) **L19**HfMe$_2$ at 25 °C; b) [**L19**HfMe]$^+$[B(C$_6$F$_5$)$_4$]$^-$ at 25 °C and c) [**L19**HfMe]$^+$[B(C$_6$F$_5$)$_4$]$^-$ at –10 °C, [D$_8$]toluene. Intense signals at ca. 7.05 ppm are due to side product CH_3CPh_3 aromatic protons that are exacerbated by poor solubility of ion pairs.

Density Functional Studies

Density functional theory calculations were used to generate geometries needed for interpretation of ROESY data, and to examine the effect of ligand structure on the relative energies of *fac*/*fac*, *fac*/*mer,* and *mer*/*mer* arrangements. Earlier work on ONNO type systems showed that calculated cation geometries are not much affected by the presence of an anion, but the inclusion of the counterion is essential for reliable prediction of the ligand conformational preference for *fac*/*fac* vs. *mer*/*mer* arrangements.[9c] Consequently, full ion pair models were investigated for select [**L**HfMe]$^+$[B(C_6F_5)$_4$]$^-$ complexes.[17]

DFT calculations were carried out at the M062X/cc-pVTZ-(-PP),PCM(Toluene)//TPSSh/SVP-LANL2DZ level using Gaussian 09; for further details see the Experimental section. Cited energies are free energies.

As found earlier for ONNO systems,[9a] geometry optimization of 5-coordinate species **L**MMe$^+$ starting from a *fac*/*fac* ligand conformation results in most cases in a rearrangement to an approximately square pyramidal (SPy) coordination geometry which could be thought of as *mer*/*mer* with one apical site empty. Substantial flexibility was observed and the ligand substitution pattern was found to have a significant effect on the preferred conformation of the [**L**HfMe]$^+$[B(C_6F_5)$_4$]$^-$ ion pairs.

DFT results indicate that [**L1**HfMe]$^+$[B(C_6F_5)$_4$]$^-$ prefers a 5-coordinate SPy structure without any direct Hf-anion contacts (Figure 17). A *mer*/*mer* complex with a short Hf-F contact, akin to earlier ONNO results, was found to be +8.7 kcal/mol higher in energy whereas a *fac*/*fac* complex in which Hf interacts with a *para*-F of the anion was predicted to be only 1.9 kcal/mol above the lowest-energy arrangement.

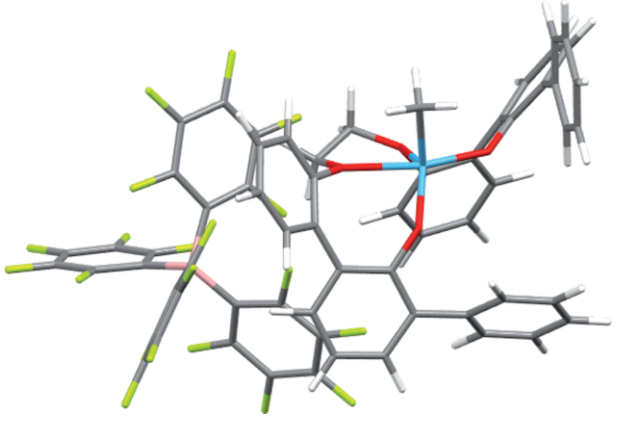

Figure 17. Optimized SPy structure of [**L1**HfMe]$^+$[B(C_6F_5)$_4$]$^-$.

Growing the ether backbone chain by one methylene unit changes the structural preference: for [**L2**HfMe]$^+$[B(C_6F_5)$_4$]$^-$ a *mer*/*mer* arrangement with a weak Hf-F interaction was found to be lowest in energy (Figure 18). A SPy geometry is slightly higher in energy (+1.0 kcal/mol) while the *fac*/*fac* structure comes in at +4.0 kcal/mol relative to *mer*/*mer*. In any case, calculations including the counterion indicate that for both [**L1**HfMe]$^+$ and [**L2**HfMe]$^+$, conformations *other than fac*/*fac* are preferred. Inspection of the corresponding *fac*/*mer* and *mer*/*mer* geometries reveals reduced distances between Hf-CH_3 and the backbone chain (relative to the *fac*/*fac* structure), consistent with the observed 2D ROESY data.

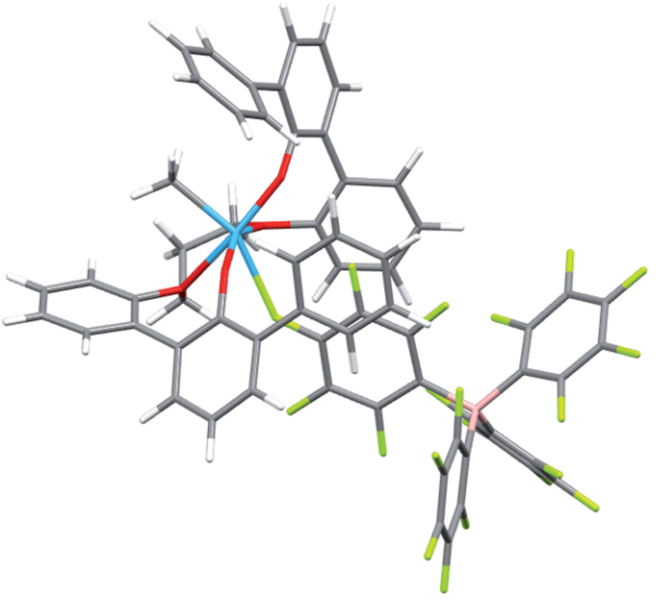

Figure 18. Optimized *mer*/*mer* structure of [**L2**HfMe]$^+$[B(C_6F_5)$_4$]$^-$.

In contrast with the above results for "small" ligands, the bulkier [**L17**HfMe]$^+$[B(C_6F_5)$_4$]$^-$ was found to prefer a *fac*/*fac* coordination mode (Figure 19) over SPy by +2.3 kcal/mol while a *mer*/*mer* structure was less favorable at +6.4 kcal/mol. Inspection of the geometries shows that, compared to the phenyl rings in **L2**, the carbazole rings in **L17** show increased steric crowding in both SPy and *mer*/*mer* geometries due to the large flat substituents. It stands to reason that **L19**, containing additional *t*Bu groups, would suffer from similar or greater steric crowding in SPy or *mer*/*mer* geometries, and hence would also prefer *fac*/*fac* ligand coordination. Thus, the DFT results support the conclusion based on NMR that [**L19**HfMe]$^+$[B(C_6F_5)$_4$]$^-$ remains *fac*/*fac* after activation.

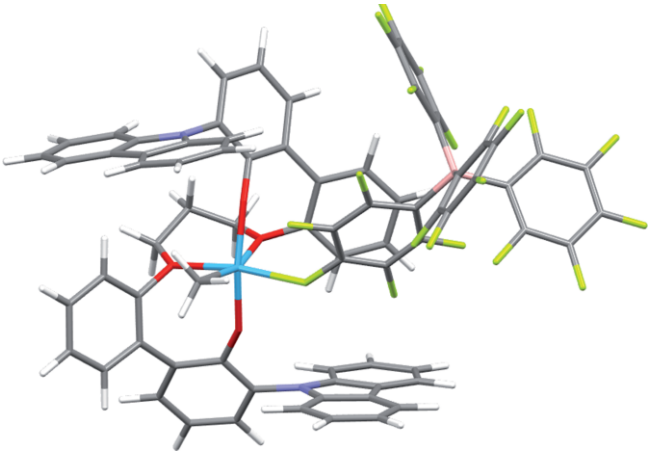

Figure 19. Optimized *fac*/*fac* structure of [**L17**HfMe]$^+$[B(C_6F_5)$_4$]$^-$.

Energies of the Zr ion-pairs demonstrated similar but more drastic results: structural rearrangement to a polymerization inactive structure is less favorable for Zr than its Hf congener (see

Tables S1–S6). These results suggest that differences in observed activities between the two metals may be influenced to some extent by differing conformational equilibria.

DFT calculations were also performed to investigate potential structures of phosphine oxide adducts formed in trapping experiments. For computational efficiency, $OPPh_3$ was modeled with $OPMe_3$ while the anion was excluded. Only *fac*/*fac* and *fac*/*mer* geometries compatible with the NMR data (i.e. that would not show a ROESY contact between Hf-CH_3 and the backbone) were considered.

Both [**L1**HfMe•$OPMe_3$]$^+$ and [**L2**HfMe•$OPMe_3$]$^+$ were found to clearly prefer *fac*/*fac* structures (Figure 20, Figure 21) over the *fac*/*mer* alternatives (by +4.4 and +5.5 kcal/mol, respectively), which again provides some support for the conclusion based on NMR data that the $OPPh_3$ adducts have *fac*/*fac* structures. This also demonstrates that caution needs to be exercised in interpreting trapping experiments: the "trapped" complex may have a structure different from the actual active species before trapping.

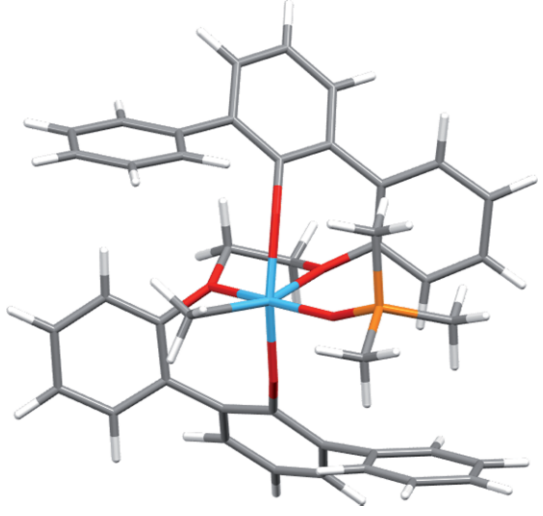

Figure 20. Optimized *fac*/*fac* structure of [**L1**HfMe•$OPMe_3$]$^+$.

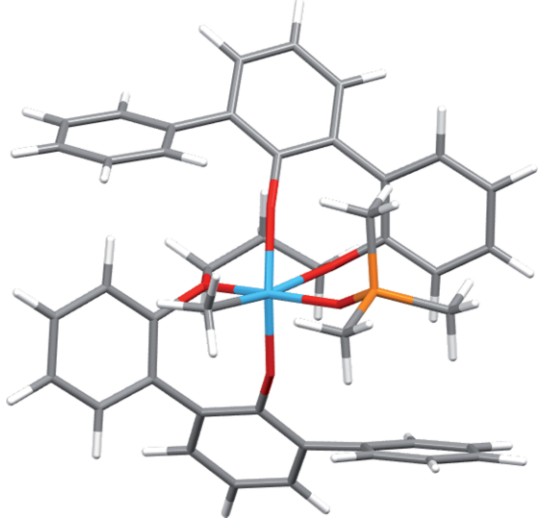

Figure 21. Optimized *fac*/*fac* structure of [**L2**HfMe•$OPMe_3$]$^+$.

Implications for Activity

Rearrangement upon activation is undesirable. In the *mer*/*mer* geometry, the catalyst is dormant as the alkyl chain and empty site are not *cis* and hence unable to undergo migratory insertion by the Cossee mechanism.[8] While propagation is in principle still possible in the *fac*/*mer* geometry, we believe it is unlikely to be as easy as in the *fac*/*fac* arrangement. Therefore, catalysts such as the carbazole-bearing systems **L17**–**L20**, for which the cations prefer *fac*/*fac* geometries, are likely to have the advantage. Control over catalyst conformation should be taken into account when designing improved catalysts, similar to what has been established for ONNO and OSSO systems.[7c,9]

Conclusions

The apparently simple chemistry of generating activated O4 catalysts is in reality not so simple. Reactions of MBn_4 with the free ligands **L**H_2 produce both monomeric and dimeric products (and possibly higher aggregates). Concentration, temperature and ligand structure all affect the course of the reaction. Reactions with MMe_4 are somewhat cleaner but also here dimeric products can be formed. It is not clear at present what would happen with dimeric precursor complexes under polymerization conditions.

Activation of **L**MMe_2 precursors with TTFB results in (mostly) clean formation of fluxional cations **L**MMe^+; NMR results indicate rearrangement of the ligand coordination geometry away from *fac*/*fac* for **L2**HfMe$^+$ but not for **L19**MMe^+. Both **L1**HfMe$^+$ and **L2**HfMe$^+$ could be trapped with $OPPh_3$ although these adducts may not be representative of the true active species. Gratifyingly, DFT results for [**L**HfMe]$^+$[$B(C_6F_5)_4$]$^-$ and [**L**HfMe•OPR_3]$^+$ are consistent with conclusions based on NMR data. For related ONNO systems, the significant energy preference for a *mer*/*mer* resting state contributes to the relatively modest activity of these catalysts.[9c] For the O4 systems studied here, the energy preference for alternative structures (such as SPy or *mer*/*mer*) appears to be less pronounced and should therefore have a smaller impact on catalyst performance.

Experimental Section

General: All reactions were performed in an inert atmosphere (nitrogen or argon), using a glove box or Schlenk techniques. All reaction and chromatography solvents were purchased from either Sigma-Aldrich, Fisher Scientific or ACROS. Deuterated solvents for NMR were purchased from Sigma-Aldrich or Cambridge Isotopes. All non-halogenated solvents required for inert conditions were purified by distillation over Na/benzophenone under an argon atmosphere. All halogenated organic solvents required for inert conditions were distilled from CaH_2 under an argon atmosphere to dry; 3 freeze-pump-thaw cycles with argon were performed to remove oxygen. Deionized water (dH_2O) underwent 3 freeze-pump-thaw cycles to remove oxygen for Suzuki coupling reactions unless otherwise noted. Inorganic and organic compounds were ordered from Sigma-Aldrich, Fisher Scientific, ACROS or Combi-Blocks and used as received unless otherwise noted. Silica gel used for column chromatography was purchased from ACROS (60 Å, 230–435 mesh). NMR spectra were acquired on a Bruker Avance III 300, 400 or 500

with spectra referenced to TMS (0 ppm) via residual solvent signals.[18] Variable temperature NMR spectra were acquired on a Bruker Avance III 500 equipped with a BCU. The following gives general procedures for the various syntheses; precise details for individual compounds (yields, characterization etc.) can be found in the Supporting Information.

Synthesis of 2: One equivalent of 2-bromophenol and 1.5 equivalents of K_2CO_3 are combined in DMF (ca. 1 M) with stirring for 15 minutes prior to addition of 1.1 equivalents of benzyl bromide or methyl iodide. The reaction is monitored by TLC and quenched with water when complete. The organic phase is washed with 2 × 10 % (w/v) $NaOH_{(aq.)}$, 3 × dH_2O, brine and then dried with $MgSO_4$. The solvent is removed under reduced pressure to yield a crude product that is purified by triturating with cold hexanes or by silica gel chromatography.

Synthesis of 3. $Pd(PPh_3)_4$ Catalyst: One equivalent of **2**, 1.8 equivalents of K_2CO_3 and 1.2 equivalents of aryl boronic acid are dissolved in degassed 10:1 DME:dH_2O under argon. 5–10 mol-% of $Pd(PPh_3)_4$ is added under a flow of argon and the mixture is refluxed over ca. 12 hours with conversion monitored by TLC. The mixture is acidified with 10 % HCl v/v and extracted with Et_2O. The organic layer is washed with dH_2O, brine and dried with $MgSO_4$. The crude product obtained by solvent removal under reduced pressure is purified by silica gel chromatography.

Synthesis of 3. $Pd_2(dba)_3$/P(*t*Bu)$_3$ Catalyst (for Sterically Hindered Coupling Reactions). In a glove box, 2.5 mol-% of $Pd_2(dba)_3$ and 3.3 equivalents of CsF are added to a Schlenk flask. The flask is moved to a Schlenk line where one equivalent of **2**, 1.2 equivalents of aryl boronic acid (e.g. 2,6-dimethylphenylboronic acid) and 6 mol-% of $[HP(tBu)_3][BF_4]$ are added under a flow of argon. Dry THF is added and the mixture is heated with vigorous stirring at 55 °C overnight or until complete. The mixture is diluted with Et_2O, filtered and the solvent is removed under reduced pressure. The crude product is purified by passing it through a plug of silica gel (eluting with hexanes) or by silica gel chromatography.

Synthesis of 4, PG = Bn: A previously published procedure is followed using **3** as the starting material.[5a]

Synthesis of 4, PG = Me: One equivalent of **3** is dissolved in dry DCM and cooled to 0 °C under argon. Three equivalents of 1 M BBr_3 in DCM are added dropwise via an addition funnel and the mixture is slowly warmed to room temperature. The reaction is carefully quenched with *i*PrOH then neutralized with saturated $NaHCO_{3(aq.)}$. The organic layer is washed with dH_2O and brine and dried with Na_2SO_4 before solvent removal under reduced pressure. The already rather pure crude product can be triturated with cold hexanes for further purification.

Synthesis of 5: In an argon atmosphere, one equivalent of **4** is dissolved in $CHCl_3$ and cooled. A freshly prepared solution of *t*BuNHBr[19] in $CHCl_3$ (one equivalent) is then added dropwise via an additional funnel; the best *ortho* selectivity is obtained while maintaining the reaction at ca. –25 °C. The reaction is carefully neutralized with saturated $NaHCO_{3(aq.)}$, the organic layer is obtained and washed with dH_2O, brine and dried with Na_2SO_4. The solvent is removed under reduced pressure to obtain a crude product that is purified by trituration with cold hexanes, by silica gel chromatography or used directly in the next step.

Synthesis of 7: 2.1 equivalents of 2-bromophenol and four equivalents of K_2CO_3 are combined in DMF with stirring for 30 minutes. One equivalent of either a) ethylene di(*p*-toluenesulfonate); b) 1,3-dibromopropane or c) 1,4-dibromobutane is added and the mixture is stirred at room temperature for 16 hours. The reaction is quenched with water and the organic phase is extracted with Et_2O. The organic phase is washed with 2 × 10 % (w/v) $NaOH_{(aq.)}$, 3 × dH_2O, brine and then dried with $MgSO_4$. The solvent is removed under reduced pressure and the crude product is purified by recrystallization from hexanes or petroleum ether, forming white needles.

Synthesis of 8: A previously published procedure[5a] is followed, substituting $B(OiPr)_3$ and 2.5 M *n*BuLi/hexanes for $B(OMe)_3$ and 1.6 M *n*BuLi/hexanes, respectively, using **7** as the starting material.

Synthesis of 9 and LH_2: A procedure similar to that used for **3** was followed ($Pd(PPh_3)_4$ catalyst) using one equivalent of **8** and two equivalents of **6**. The crude product is purified by silica gel chromatography and deprotected similar to **4**/**6**, using 10 % (w/w) of Pd/C per Bn group.

Synthesis of 10: One equivalent of 2-halophenol and 1.5 equivalents of DHP are dissolved in dry DCM under argon. The mixture is cooled to 0 °C and 2 mol-% of PPTS is added under a flow of argon. The reaction is allowed to slowly warm to room temperature and is monitored by TLC – extra DHP and PPTS is added as necessary to ensure conversion. The reaction is quenched with 10 % (w/v) NaOH and the organic layer is washed with dH_2O, brine and dried with $MgSO_4$. Solvent is removed under reduced pressure and the crude product is placed under high vacuum to remove residual DHP, yielding a pure golden oil.

Synthesis of 11 for Pd Catalyzed Reactions: A procedure similar to the synthesis of **3** is followed where R-Nu is R-$B(OH)_2$, and excluding H^+ addition at any step to prevent THP cleavage. The crude product is purified by silica gel chromatography.

Synthesis of 11 for Cu Catalyzed Reactions: A previously published procedure is followed using **10** (X=I) and R1-Nu being carbazole or its *t*-butylated derivative.[4] The crude product is purified by silica gel chromatography or by recrystallization from CH_3CN.

Synthesis of 12*:* A previously published procedure is followed using **11** as the starting material.[4]

Synthesis of LH_2, Method B: One equivalent of **7**, 2.2 equivalents of **12** and 3.3 equivalents of K_2CO_3 are dissolved in degassed 10:1 DME:dH_2O under argon. 10 mol-% of $Pd(PPh_3)_4$ is added under a flow of argon and the mixture is heated at reflux over ca. 12 hours; progress is monitored by TLC. Once the reaction is complete, 20 % (w/v) HCl is added and the mixture is refluxed until THP is cleaved. The mixture is diluted with EtOAc and the organic layer is washed with dH_2O, brine and dried with Na_2SO_4. The solvent is removed under reduced pressure and the crude product is purified by silica gel chromatography or recrystallization from CH_3CN.

Synthesis of LH_2, Method B': 2.1 equivalents of **11** are dissolved in dry THF under argon and cooled to 0 °C. 2.31 equivalents of 1.6 M *n*BuLi in hexanes are added dropwise and the mixture is stirred at 0 °C for three hours. 2.52 equivalents of anhydrous $ZnCl_2$ are added under a flow of argon, resulting in a color change and reduced turbidity. The mixture is slowly warmed to room temperature and stirred for an additional hour. One equivalent of **7** and 5 mol-% of $Pd(PPh_3)_4$ are added under a flow of argon and the reaction is heated at reflux overnight. Completion is checked by TLC. 20 % HCl (v/v) is added and the mixture is again refluxed until hydrolysis of THP is complete as monitored by TLC. The contents are extracted with EtOAc, the solvent is removed under reduced pressure and the crude product is purified by silica gel chromatography or recrystallization from CH_3CN.

LMBn_2 Synthesis – NMR Scale: Approximately 15–30 mg of **L**H_2 is dissolved in [D_6]benzene or [D_8]toluene (approximately 0.5 mL) in a glove box under N_2. The contents are combined with one equiva-

lent of MBn_4, mixed and immediately taken for NMR analysis. The mixture is heated at 60 °C if necessary until **L**H_2 consumption is complete, monitoring the O*H* signals of the ligand.

L2/$HfBn_4$ complexation experiments.

Variation 1: 76.1 mg of $HfBn_4$ is dissolved in 5 mL of toluene (28 mM) in a Schlenk tube. The tube is covered with Al foil and cooled to –78 °C on the Schlenk line. Under a flow of argon, 79.1 mg of **L2**H_2 is added in one portion. The mixture is stirred at –78 °C for 30 minutes. The cold bath is removed and the mixture is slowly warmed to room temperature. The solvent is removed under reduced pressure to yield a white, poorly soluble powder that is not purified prior to NMR analysis to avoid affecting the dimer/monomer ratio.

Variation 2: 72.2 mg of $HfBn_4$ is dissolved in 2.5 mL of toluene in one Schlenk tube covered with Al foil and 75.6 mg of **L2**H_2 is dissolved in 2.5 mL of toluene in another tube. Both are heated in an oil bath to 65 °C on a Schlenk line. The **L2** solution is quickly added to the $HfBn_4$ solution (26 mM final concentration) using a syringe. The mixture is cooled and the solvent is removed under reduced pressure to yield a white, crystalline powder that is not purified prior to NMR analysis to avoid affecting the dimer/monomer ratio.

Variation 3: 60.0 mg of $HfBn_4$ is dissolved in 9 mL of toluene in a vial equipped with a stir bar. The vial is cooled to –35 °C for one hour and 62.4 mg of **L2**H_2 is added in one portion with stirring. The mixture is slowly warmed to room temperature, resulting in a color change from pale-yellow to colorless. The solvent is removed under reduced pressure, yielding 107 mg of a white powder. Crystals of (μ-**L2**)$_2$[$HfBn_2$]$_2$ suitable for XRD are grown from a toluene solution of the crude product at –35 °C.

LMMe$_2$ Synthesis: A slurry of ca. 40–160 mg of MCl_4 in approximately 10–15 mL of toluene in a 20 mL vial equipped with a stir bar is cooled to –35 °C in a glove box freezer. The vial is removed and immediately four equivalents of 3 M MeMgBr in Et_2O are added. The mixture is stirred for 3–10 minutes or until a yellowish colour is observed. One equivalent of **L**H_2 is added as a solid, resulting in the immediate release of CH_4. The solution darkens on warming. After at least one hour of stirring (after the **L**H_2 addition), the solvent is removed under reduced pressure. The dark residue is mixed with toluene, filtered through a PE filter frit and the solvent is again removed under reduced pressure, yielding a white or light tan crystalline solid that according to ^{1}H NMR is of high purity.

Activation Studies: About 15–20 mg of precatalyst **L**$HfMe_2$ is dissolved in approximately 0.5 mL of [D_8]toluene and analyzed by NMR before activation. An equimolar amount of $[CPh_3]^+[B(C_6F_5)_4]^-$ is added directly to the tube, resulting in separation of a dense, dark orange oil. The mixture is vortexed and quickly inserted in the NMR spectrometer stabilized at the desired starting temperature.

OPPh$_3$ Trapping: One equivalent of $OPPh_3$ is added directly to the NMR tube containing [**L**HfMe]$^+$[$B(C_6F_5)_4$]$^-$, vortexed and taken immediately for analysis. The reaction of $OPPh_3$ with [**L1**HfMe]$^+$-[$B(C_6F_5)_4$]$^-$ was slow and contents were stored in a glove box overnight. The [D_8]toluene was decanted from the orange oil which was then diluted with additional [D_8]toluene, vortexed and taken for analysis.

Single-Crystal X-ray Structure Determinations: Ligand crystals suitable for X-ray diffraction were grown from: a) silica gel chromatography fractions at room temperature; b) slow evaporation of $CDCl_3$ at room temperature or c) a $CDCl_3$ solution layered with hexanes at room temperature. Crystals of metal complexes suitable for X-ray diffraction were grown in an N_2 atmosphere from: a) a saturated toluene solution cooled to –35 °C; b) a toluene solution layered with hexanes at room temperature; c) a benzene solution with slow evaporation at room temperature or d) a benzene solution layered with hexanes at room temperature; the latter method is particularly successful for producing high-quality crystals for these types of complexes. Crystals were covered with Parabar oil, loaded onto a nylon loop and cooled in a 150 K stream of N_2 on a Bruker D8 Quest ECO CMOS diffractometer.

CCDC 1918161 (for **9a-2**), 1918162 (for **9b-2**), 1918163 (for **9b-3**), 1918164 (for **L16**$HfBn_2$), 1918165 (for **L16**$HfMe_2$), 1918166 (for **L17**$HfMe_2$), 1918167 (for **L18**$HfMe_2$), 1918168 (for **L18**), 1918169 (for **L19**$HfMe_2$), 1918170 (for **L19**$ZrMe_2$), 1918171 (for **L1**$HfMe_2$), 1918172 (for **L1**$ZrMe_2$), 1918173 (for **L1**), 1918174 (for (μ-**L20**)$_2$-[$HfBn_2$]$_2$), 1918175 (for (μ-**L2**)$_2$[$HfBn_2$]$_2$), 1918176 (for **L2**$HfBn_2$), 1918177 (for **L2**$HfMe_2$), 1918178 (for **L2**$ZrMe_2$), 1918179 (for **L3**$ZrMe_2$), 1918180 (for **L5**$ZrMe_2$), 1918181 (for **L6**ZrBn2) and 1918182 (for **L7**ZrBn2) contain the supplementary crystallographic data for this paper. These data can be obtained free of charge from The Cambridge Crystallographic Data Centre.

Computational Studies: Density-functional calculations were carried out with Gaussian 09.[20] Geometries were optimized at the TPSSh[21]/SVP[22]-LANL2DZ[23] level, (small-core ECP at Zr/Hf) using an external optimizer.[24] Vibrational analyses were carried out to verify the nature of all stationary points. Improved single-point energies were obtained at M062X[25]/cc-pVTZ(-PP)[26] with a PCM(Toluene)[27] solvent correction. The cc-pVTZ basis sets were downloaded from the EMSL basis set exchange.[28] The single-point energies were then combined with thermal corrections (enthalpy and entropy, 298 K, 1 bar) to obtain final free energies; entropy corrections were scaled by 0.67 to account for reduced freedom of movement in solution.[29] Calculations on the full system [**L19**HfMe]$^+$[$B(C_6F_5)_4$]$^-$ were not feasible so the smaller ligand **L17** was used as a model for **L19**.

Supporting Information (see footnote on the first page of this article): Procedures for syntheses of ligands and precatalysts; NMR spectra; DFT calculated energies and free energies; xyz archives of geometries.

Acknowledgments

This work is part of the Research Programme of the Dutch Polymer Institute DPI, Eindhoven, The Netherlands, project nr. #791. We thank Cristiano Zuccaccia for valuable advice for activation chemistry studies, Christian Ehm for valuable discussion of DFT studies, Emy Komatsu for HRMS measurements, Mark Cooper for X-ray crystallography, David Davidson for diffusion NMR experiments and Bill Bressenel for elemental analysis. DEH thanks NSERC (RGPIN-2014–03733), and the Canada Foundation for Innovation and Research Manitoba for funding in support of an X-ray diffractometer (#32146).

Keywords: Coordination modes · Hafnium · Olefin polymerization · Zirconium

[1] J. R. Severn, in *Multimodal Polymers with Supported Catalysts: Design and Production* (Eds.: A. R. Albunia, F. Prades, D. Jeremic), Springer International Publishing, Cham, **2019**, pp. 1–53.
[2] S. Ali, *The Catalyst Review* **2014**, *27*, 7-14. Accessed via https://users.wpi.edu/~jlwilcox/documents/CatalystReview-04-2014-Wilcox.pdf.

[3] T. R. Boussie, O. Brummer, G. M. Diamond, C. Goh, A. M. LaPointe, M. K. Leclerc, J. A. W. Shoemaker (Ed.: U. S. P. Office), *Symyx Technologies*, Inc. (Santa Clara, CA) US, **2003**.
[4] J. Klosin, P. J. Thomas, R. D. Froese, X. Cui, *Vol. US **2011**/0282018 A1* (Ed. USPO), Dow Global Technologies, **2011**.
[5] a) E. T. Kiesewetter, S. Randoll, M. Radlauer, R. M. Waymouth, *J. Am. Chem. Soc.* **2010**, *132*, 5566–5567; b) S. Randoll, E. T. Kiesewetter, R. M. Waymouth, *J. Polym. Sci., Part A J. Pol. Sci. A Pol. Chem.* **2012**, *50*, 2604–2611; c) E. T. Kiesewetter, R. M. Waymouth, *Macromolecules* **2013**, *46*, 2569–2575.
[6] a) E. Y. Tshuva, I. Goldberg, M. Kol, *J. Am. Chem. Soc.* **2000**, *122*, 10706–10707; b) E. Y. Tshuva, I. Goldberg, M. Kol, *J. Am. Chem. Soc.* **2001**, *123*, 3621–3621.
[7] a) A. Ishii, T. Toda, N. Nakata, T. Matsuo, *J. Am. Chem. Soc.* **2009**, *131*, 13566–13567; b) N. Nakata, T. Toda, T. Matsuo, A. Ishii, *Inorg. Chem.* **2012**, *51*, 274–281; c) A. Ishii, K. Ikuma, N. Nakata, K. Nakamura, H. Kuribayashi, K. Takaoki, *Organometallics* **2017**, *36*, 3954–3966.
[8] P. Cossee, *Tetrahedron Lett.* **1960**, *1*, 12–16.
[9] a) G. Ciancaleoni, N. Fraldi, P. H. M. Budzelaar, V. Busico, A. Macchioni, *Dalton Trans.* **2009**, 8824–8827; b) G. Ciancaleoni, N. Fraldi, P. H. M. Budzelaar, V. Busico, A. Macchioni, *Organometallics* **2011**, *30*, 3096–3105; c) G. Ciancaleoni, N. Fraldi, R. Cipullo, V. Busico, A. Macchioni, P. H. M. Budzelaar, *Macromolecules* **2012**, *45*, 4046–4053.
[10] To be published.
[11] a) S. E. Reybuck, A. L. Lincoln, S. Ma, R. M. Waymouth, *Macromolecules* **2005**, *38*, 2552–2558; b) A. Cohen, G. W. Coates, M. Kol, *J. Polym. Sci., Part A J. Pol. Sci. A Pol. Chem.* **2013**, *51*, 593–600; c) N. Nakata, T. Toda, T. Matsuo, A. Ishii, *Macromolecules* **2013**, *46*, 6758–6764; d) J. Sampson, G. Choi, M. N. Akhtar, E. A. Jaseer, R. Theravalappil, H. A. Al-Muallem, T. Agapie, *Organometallics* **2017**, *36*, 1915–1928; e) E. Y. Tshuva, S. Groysman, I. Goldberg, M. Kol, Z. Goldschmidt, *Organometallics* **2002**, *21*, 662–670; f) S. Groysman, I. Goldberg, M. Kol, E. Genizi, Z. Goldschmidt, *Inorg. Chim. Acta* **2003**, *345*, 137–144; g) C.-C. Liu, L.-C. So, J. C. Y. Lo, M. C. W. Chan, H. Kaneyoshi, H. Makio, *Organometallics* **2012**, *31*, 5274–5281; h) H. Tsurugi, Y. Matsuo, T. Yamagata, K. Mashima, *Organometallics* **2004**, *23*, 2797–2805; i) R. C. Klet, C. N. Theriault, J. Klosin, J. A. Labinger, J. E. Bercaw, *Macromolecules* **2014**, *47*, 3317–3324; j) S. Dagorne, S. Bellemin-Laponnaz, C. Romain, *Organometallics* **2013**, *32*, 2736–2743; k) R. P. Kamalesh Babu, R. McDonald, S. A. Decker, M. Klobukowski, R. G. Cavell, *Organometallics* **1999**, *18*, 4226–4229; l) J. C. Y. Lo, M. C. W. Chan, P.-K. Lo, K.-C. Lau, T. Ochiai, H. Makio, *Organometallics* **2013**, *32*, 449–459; m) I. E. Nifant'ev, P. V. Ivchenko, V. V. Bagrov, S. M. Nagy, L. N. Winslow, J. A. Merrick-Mack, S. Mihan, A. V. Churakov, *Dalton Trans.* **2013**, *42*, 1501–1511.
[12] M. R. Radlauer, T. Agapie, *Organometallics* **2014**, *33*, 3247–3250.
[13] a) R. F. Jordan, R. E. LaPointe, N. Baenziger, G. D. Hinch, *Organometallics* **1990**, *9*, 1539–1545; b) M. Bochmann, S. J. Lancaster, *Organometallics* **1993**, *12*, 633–640; c) C. Pellecchia, A. Immirzi, D. Pappalardo, A. Peluso, *Organometallics* **1994**, *13*, 3773–3775.
[14] J. Klosin, in *4th Blue Sky Conference on Catalytic Olefin Polymerization*, Sorrento, Italy, **2016**.
[15] L. Jia, X. Yang, C. L. Stern, T. J. Marks, *Organometallics* **1997**, *16*, 842–857.
[16] The minor component appears to show only two ether signals at higher temperatures. HSQC suggests that these two ether protons are bound to the same carbon, suggesting effective C_2 symmetry: this might be the *fac/fac* isomer but the crowded nature of the spectrum precludes assignment for the minority species.
[17] An exhaustive search of possible ion pair geometries was not feasible for the larger ligands, so it is possible some low-energy arrangements have been missed.
[18] G. R. Fulmer, A. J. M. Miller, N. H. Sherden, H. E. Gottlieb, A. Nudelman, B. M. Stoltz, J. E. Bercaw, K. I. Goldberg, *Organometallics* **2010**, *29*, 2176–2179.
[19] S. N. Georgiades, J. Clardy, *Org. Lett.* **2005**, *7*, 4091–4094.
[20] M. J. Frisch, G. W. Trucks, H. B. Schlegel, G. E. Scuseria, M. A. Robb, J. R. Cheeseman, G. Scalmani, V. Barone, B. Mennucci, G. A. Petersson, H. Nakatsuji, M. Caricato, X. Li, H. P. Hratchian, A. F. Izmaylov, J. Bloino, G. Zheng, J. L. Sonnenberg, M. Hada, M. Ehara, K. Toyota, R. Fukuda, J. Hasegawa, M. Ishida, T. Nakajima, Y. Honda, O. Kitao, H. Nakai, T. Vreven, J. A. Montgomery Jr., J. E. Peralta, F. Ogliaro, M. Bearpark, J. J. Heyd, E. Brothers, K. N. Kudin, V. N. Staroverov, R. Kobayashi, J. Normand, K. Raghavachari, A. Rendell, J. C. Burant, S. S. Iyengar, J. Tomasi, M. Cossi, N. Rega, J. M. Millam, M. Klene, J. E. Knox, J. B. Cross, V. Bakken, C. Adamo, J. Jaramillo, R. Gomperts, R. E. Stratmann, O. Yazyev, A. J. Austin, R. Cammi, C. Pomelli, J. W. Ochterski, R. L. Martin, K. Morokuma, V. G. Zakrzewski, G. A. Voth, P. Salvador, J. J. Dannenberg, S. Dapprich, A. D. Daniels, Ö. Farkas, J. B. Foresman, J. V. Ortiz, J. Cioslowski, D. J. Fox, *Gaussian 09, Revision B.01*, Gaussian, Inc., Wallingford CT, **2009**.
[21] a) V. N. Staroverov, G. E. Scuseria, J. Tao, J. P. Perdew, *J. Chem. Phys.* **2003**, *119*, 12129–12137; b) J. M. Tao, J. P. Perdew, V. N. Staroverov, G. E. Scuseria, *Phys. Rev. Lett.* **2003**, *91*, 146401.
[22] K. Eichkorn, O. Treutler, H. Ohm, M. Haser, R. Ahlrichs, *Chem. Phys. Lett.* **1995**, *242*, 652–660.
[23] P. J. Hay, W. R. Wadt, *J. Chem. Phys.* **1985**, *82*, 270–283.
[24] a) J. Baker, *J. Comput. Chem.* **1986**, *7*, 385–395; b) J. Baker, K. Wolinski, M. Malagoli, D. Kinghorn, P. Wolinski, G. Magyarfalvi, S. Saebo, T. Janowski, P. Pulay, *J. Comput. Chem.* **2009**, *30*, 317–335.
[25] Y. Zhao, D. G. Truhlar, *Theor. Chem. Acc.* **2008**, *120*, 215–241.
[26] a) T. H. Dunning, *J. Chem. Phys.* **1989**, *90*, 1007–1023; b) K. A. Peterson, D. Figgen, M. Dolg, H. Stoll, *J. Chem. Phys.* **2007**, *126*, 124101; c) D. Figgen, K. A. Peterson, M. Dolg, H. Stoll, *J. Chem. Phys.* **2009**, *130*, 164108.
[27] a) S. Miertus, E. Scrocco, J. Tomasi, *Chem. Phys.* **1981**, *55*, 117–129; b) S. Miertuš, J. Tomasi, *Chem. Phys.* **1982**, *65*, 239–245; c) J. Tomasi, B. Mennucci, R. Cammi, *Chem. Rev.* **2005**, *105*, 2999–3093; d) G. Scalmani, M. J. Frisch, *J. Chem. Phys.* **2010**, *132*, 114110.
[28] a) K. L. Schuchardt, B. T. Didier, T. Elsethagen, L. S. Sun, V. Gurumoorthi, J. Chase, J. Li, T. L. Windus, *J. Chem. Inf. Model.* **2007**, *47*, 1045–1052; b) D. Feller, *J. Comput. Chem.* **1996**, *17*, 1571–1586.
[29] a) R. Raucoules, T. de Bruin, P. Raybaud, C. Adamo, *Organometallics* **2009**, *28*, 5358–5367; b) S. Tobisch, T. Ziegler, *J. Am. Chem. Soc.* **2004**, *126*, 9059–9071.

Received: July 2, 2019